Regional synapse gain and loss accompany memory formation in larval zebrafish

William P. Dempsey[a,1], Zhuowei Du[a,1], Anna Nadtochiy[b], Colton D. Smith[a], Karl Czajkowski[c], Andrey Andreev[b], Drew N. Robson[d], Jennifer M. Li[d], Serina Applebaum[a], Thai V. Truong[b], Carl Kesselman[c,e], Scott E. Fraser[a,b], and Don B. Arnold[a,2]

[a]Department of Biological Sciences, Division of Molecular and Computational Biology, University of Southern California, Los Angeles, CA 90089; [b]Translational Imaging Center, University of Southern California, Los Angeles, CA 90089; [c]Information Sciences Institute, University of Southern California, Los Angeles, CA 90292; [d]Systems Neuroscience & Neuroengineering, Max Planck Institute for Biological Cybernetics, 72076 Tübingen, Germany; and [e]Daniel J. Epstein Department of Industrial and Systems Engineering, Viterbi School of Engineering, University of Southern California, Los Angeles, CA 90089

Edited by Bernardo Sabatini, Department of Neurobiology, Harvard Medical School, Boston, MA; received April 23, 2021; accepted December 3, 2021

Defining the structural and functional changes in the nervous system underlying learning and memory represents a major challenge for modern neuroscience. Although changes in neuronal activity following memory formation have been studied [B. F. Grewe et al., *Nature* 543, 670–675 (2017); M. T. Rogan, U. V. Stäubli, J. E. LeDoux, *Nature* 390, 604–607 (1997)], the underlying structural changes at the synapse level remain poorly understood. Here, we capture synaptic changes in the midlarval zebrafish brain that occur during associative memory formation by imaging excitatory synapses labeled with recombinant probes using selective plane illumination microscopy. Imaging the same subjects before and after classical conditioning at single-synapse resolution provides an unbiased mapping of synaptic changes accompanying memory formation. In control animals and animals that failed to learn the task, there were no significant changes in the spatial patterns of synapses in the pallium, which contains the equivalent of the mammalian amygdala and is essential for associative learning in teleost fish [M. Portavella, J. P. Vargas, B. Torres, C. Salas, *Brain Res. Bull.* 57, 397–399 (2002)]. In zebrafish that formed memories, we saw a dramatic increase in the number of synapses in the ventrolateral pallium, which contains neurons active during memory formation and retrieval. Concurrently, synapse loss predominated in the dorsomedial pallium. Surprisingly, we did not observe significant changes in the intensity of synaptic labeling, a proxy for synaptic strength, with memory formation in any region of the pallium. Our results suggest that memory formation due to classical conditioning is associated with reciprocal changes in synapse numbers in the pallium.

classical conditioning | zebrafish | pallium | synapse | learning and memory

It is widely believed that memories are formed as a result of alterations in synaptic connections between axons and dendrites, an idea first proposed by Ramon y Cajal (1–4). Although synapse changes have been extensively studied in brain slices in the context of long-term potentiation (5, 6), less is known about how synapses in a living vertebrate are modified when a memory is formed.

Memory formation has been widely studied using classical conditioning (CC), a robust and straightforward form of learning in which an animal is exposed to a neutral stimulus (conditioned stimulus, CS) paired with an appetitive or aversive stimulus (unconditioned stimulus, US) that evokes a specific behavioral response (UR, unconditioned response) (7, 8). As a result of the pairing, animals learn to associate the CS with the US, causing them to respond to the CS with a conditioned response (CR) identical to the UR, signifying memory retrieval (9, 10). Memory retrieval is also evoked by activating a cellular engram, a group of neurons active during memory formation and retrieval (11–18). The central locus of CC in mammals, the amygdala (19), is located in a relatively inaccessible area beneath the cortex (20). Thus, although numerous longitudinal imaging studies have documented experience-dependent changes in the structure of spines of cortical and hippocampal neurons (21, 22), few imaging studies have directly examined synaptic changes that occur in the amygdala during associative memory formation.

Instead, synaptic changes that occur in the amygdala during CC (23) have been studied primarily using indirect measures of synaptic strength, such as the ratio of α-amino-3-hydroxy-5-methyl-4-isoxazolepropionic acid receptor/N-methyl D-aspartate (AMPA/NMDA) currents in excitatory postsynaptic currents (EPSCs). Increases in AMPA/NMDA ratio in amygdalar neurons following auditory fear conditioning (FC), a type of CC (24–27), indicate that associative memory formation coincides with increases in synaptic strength. In addition, imaging experiments in brain regions beyond the amygdala have shown diverse effects following CC. For example, following contextual fear conditioning, engram neurons in the CA1 region of the hippocampus that receive inputs from CA3 engram neurons displayed spines that were larger and more densely packed than nonengram cells (28). Furthermore, experiments in which neuronal morphology was directly observed before and after FC found that neurons in the frontal association (29) and primary motor cortex (30) showed a decrease in the number of spines, whereas neurons in the auditory cortex showed an increase in spine number with memory formation (31).

To obtain previously unavailable insight into memory formation within the central locus of associative memory storage, we developed a paradigm combining in vivo labeling and imaging

Significance

Imaging of labeled excitatory synapses in the intact brain before and after classical conditioning permits a longitudinal analysis of changes that accompany associative memory formation. When applied to midlarval stage zebrafish, this approach reveals adjacent regions of synapse gain and loss in the lateral and medial pallium, respectively. Such major structural changes could account for the robust nature of memory formation from classical conditioning.

Author contributions: W.P.D., Z.D., T.V.T., S.E.F., and D.B.A. designed research; W.P.D., Z.D., and C.D.S. performed research; W.P.D., A.N., K.C., A.A., D.N.R., J.M.L., and C.K. contributed new reagents/analytic tools; Z.D., A.N., S.A., and T.V.T. analyzed data; A.A., T.V.T., and S.E.F. designed and built the SPIM and the apparatus for tail-flick conditioning; D.N.R. and J.M.L. developed methods for using heat as an unconditioned stimulus; and W.P.D. and D.B.A. wrote the paper.

The authors declare no competing interest.

This article is a PNAS Direct Submission.

[1]W.P.D. and Z.D. contributed equally to this work.

[2]To whom correspondence may be addressed. Email: darnold@usc.edu.

This article contains supporting information online at http://www.pnas.org/lookup/suppl/doi:10.1073/pnas.2107661119/-/DCSupplemental.

Published January 14, 2022.

with informatics and analysis tools. We used this paradigm to map synaptic changes that occur over time in the intact brain of a living vertebrate during memory formation. We imaged the pallium of teleost fish, which contains the putative homolog of the mammalian amygdala based on anatomy (32), gene expression (33), and function (34). The pallium is on the surface of the brain (35), and zebrafish larvae are highly transparent, allowing for intact, whole-brain imaging using selective plane illumination microscopy (SPIM) without the need for invasive intervention (36). In addition, while most studies of learning in zebrafish have used adults (37–40), at least one study showed that larval zebrafish can learn to associate a place with a positive valence US (41). These attributes suggest that larval zebrafish may be an ideal model organism for studying synaptic changes during memory formation due to CC. We have engaged this challenge by combining purpose-built experimental tools with data management software that enables transparent analyses of large and heterogeneous datasets. All data were characterized and stored at the time of creation in a customized data management system designed to conform to findability, accessibility, interoperability, and reusability (i.e., FAIR principles) (see Materials and Methods) (42).

Results

A Paradigm for CC. Electric shock–based CC does not work efficiently in zebrafish larvae (43), so we developed a CC paradigm, tail-flick conditioning (TFC), to produce associative memories in 14- to 16-d-postfertilization (dpf) zebrafish. TFC uses heating from a near-infrared laser, as in ref. 44, as the US and light from a light-emitting diode (LED) as the CS. The fish's head is immobilized in agarose, leaving the fish free to flick its tail, which is the UR and CR (Fig. 1*A* and *SI Appendix*, Fig. S1*A*). Using a custom-built behavioral apparatus (*SI Appendix*, Fig. S1*B*), we implemented induction of CC and testing in three phases, each with a distinct stimulus series: 1) habituation, exposure to the CS alone (20 rounds); 2) training, exposure to overlapping CS and US (20 rounds); and 3) testing, exposure to CS alone (5 rounds; Fig. 1 *B–D* and *SI Appendix*, Fig. S1 *C–E*).

Fish used in imaging experiments were subjected to a fourth phase, in which they were reexposed to the training regimen for 10 rounds to compensate for any extinction that might have resulted from testing (Fig. 1*B*; see Materials and Methods). Control fish were exposed to the US alone, the CS alone, or to no stimulus (NS). This TFC paradigm, which lasts ∼3 h (Fig. 1*B*), can be characterized as cued aversive conditioning.

To determine if a fish learned, tail flicking was measured using custom software (see Materials and Methods) and integrated into our data management pipeline. The baseline rate of tail flicking was determined by measuring responses to CSs during the final five rounds of habituation (before TFC), measuring flicking during five identical time intervals without a stimulus following training (random flicking), and plotting the results in a cumulative histogram (Fig. 1*E*). Measuring tail flicking during the five rounds of testing revealed that 30% of fish (4.5 to 5.0 mm) responded at least three times in response to five CSs ($n = 90$). As no fish responded more than two times under control conditions, we estimate that our learning rate is at least 30%. Fish that responded to five out of five CSs during testing were designated superlative learners (L, Fig. 1 *C–E*). Fish that responded to either three or four CSs were designated partial learners (PL, Fig. 1 *C–E*); fish that did not respond to any stimuli were designated nonlearners (NL). Fish that responded either once or twice were designated as weak learners (WL) and not used in analyses of synapses, as it was difficult to conclude unequivocally whether or not they had learned. We further evaluated the fish using the "flick ratio" (FR), which is the fraction of time spent flicking following a stimulus (see Materials

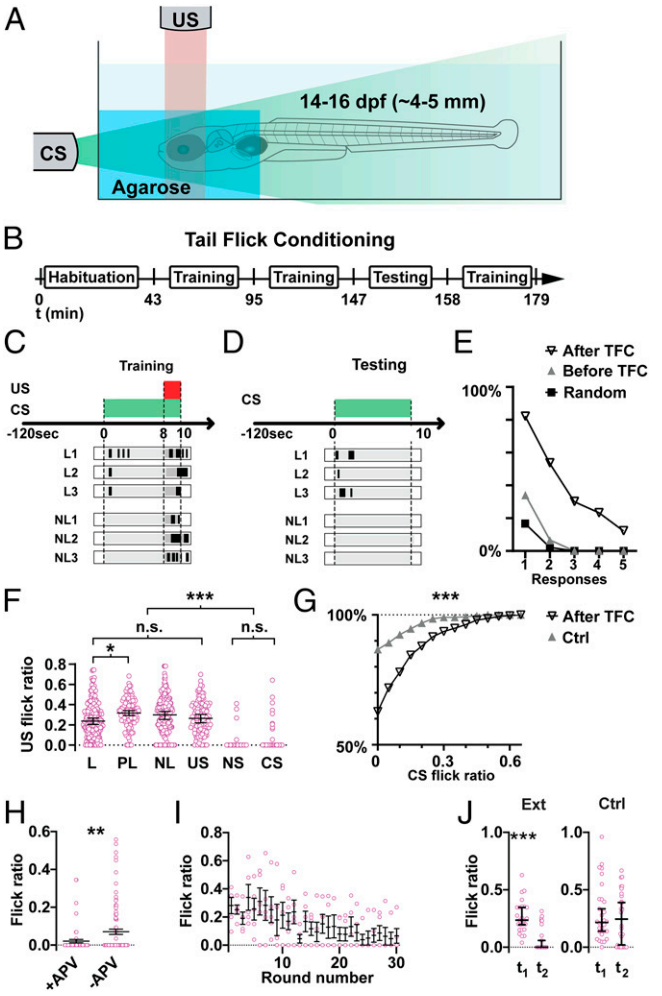

Fig. 1. Tail Flick Conditioning (TFC), a CC paradigm for larval zebrafish. (*A*) The head of the zebrafish undergoing TFC is encased in low-melt agarose, leaving the tail free to move. The CS consists of light from a green LED; the US is heat produced by an NIR laser. The CR is tail flicking. (*B*) Timeline of the TFC paradigm. (*C*) During training, fish are exposed to both the CS and US. In response to the US, all fish flicked their tails vigorously (black bars). Here, we display late-stage training rounds for three L and three NL fish. (*D*) During the testing phase of TFC, the fish is exposed to the CS alone. L respond immediately upon presentation of CS; NL do not. Here, early-stage testing rounds are shown. (*E*) Cumulative histogram of the percentage of larval zebrafish that respond with tail flicking to the five CSs presented during testing one or more times, two or more times, etc. (After TFC, inverted triangles). The baseline flicking histograms from fish during the final rounds of Habituation (Before TFC, gray triangles) or from fish assayed after TFC for five time windows when no stimulus is present (Random, filled squares) are different. (*F*) The FR (fraction of time tail is flicking) when US is presented during training are similar for L ($n = 11$ fish), PL ($n = 6$), NL ($n = 11$), and US only (US, $n = 11$) and different from the FR during the same time period for fish exposed to CS only ($n = 11$) or NS($n = 11$; $^{***}P < 0.005$, $^{*}P < 0.05$, Kruskal–Wallis test). No pairwise comparison between L, PL, NL, or US is significant except for L versus PL ($^{*}P < 0.05$, Kruskal–Wallis test). (*G*) The FR in response to the CS during testing is significantly different in fish exposed to TFC versus control fish ($^{***}P < 0.0001$, Kolmogorov–Smirnov test). Cumulative probability distributions are shown. (*H*) The FR (averaged for all fish during testing) is significantly reduced in fish exposed to 2-amino-5-phosphonovaleric acid (APV) during TFC compared to control fish ($n = 12$ fish +APV, 19 fish −APV; $^{**}P < 0.01$, Mann–Whitney *U* test). Each data point represents the response to a single presentation of the CS. (*I*) The FR diminishes over 30 presentations of CS alone (extinction, $n = 5$) in a set of L fish by ∼75%. (*J*) FR before and after extinction (Ext, t_1 and t_2) are significantly different ($^{***}P < 0.005$, $n = 5$ as in *H*, Mann–Whitney *U* test). FR at t_1, t_2 without extinction ($n = 6$) are not significantly different ($P > 0.05$, Mann–Whitney *U* test). Data available at https://doi.org/10.25551/1/1-1YZE (45).

and Methods). As expected, fish that underwent training (L, PL, WL, and NL) responded to the US with an elevated FR, whereas control fish (US, CS, and NS) not exposed to the US had a minimal FR during the same time period (Fig. 1*F*). Importantly, fish exposed to TFC ($n = 128$) responded to the CS with an FR significantly different from control fish ($n = 108$; $P < 0.0001$, Kolmogorov–Smirnov test), providing further evidence that TFC induced learning (Fig. 1*G*).

Zebrafish learning rate correlated with developmental stage: 30% of fish between 4.5 and 5.0 mm standard length (SL) were either L (12.2%) or PL (17.8%, $n = 90$); in contrast, 7.2% of fish between 4.0 and 4.5 mm were L ($n = 153$) and 18.3% were PL (*SI Appendix*, Fig. S1*F*). Learning during TFC was largely blocked by exposure of the fish to 2-amino-5-phosphonovaleric acid (APV) (Fig. 1*H*; $P < 0.01$, Mann–Whitney *U* test), suggesting a dependence of TFC learning on NMDA receptor–based synaptic plasticity. To test whether TFC is susceptible to extinction, we exposed L fish to 25 presentations of the CS alone following learning. These fish displayed a response to the CS that diminished to less than 25% of the initial response (Fig. 1*I*; $P < 0.0001$, Mann–Whitney *U* test). The responses of fish tested at a similar interval following learning, but without additional exposure to the CS, did not differ significantly from the initial response (Fig. 1*J*; $P > 0.05$, Mann–Whitney *U* test). Thus, TFC learning is NMDA receptor–dependent and can undergo extinction, both hallmarks of CC.

A Data-Centric Approach to Experimental Design. We generated the results reported in this paper using a unique data collection paradigm in which we captured all data at the point of generation. Data include all procedures performed on the fish in preparation for behavior and imaging experiments, behavioral outputs during conditioning, all raw and processed imaging data, software, and analyses produced either by humans or computational pipelines. All data were entered into an innovative data management system at the point of generation and curated with high-fidelity metadata descriptions (https://doi.org/10.25551/1/1-1JR0) (46). Metadata models and any relationships between different types of data were described using an explicit data model that was captured as the model adapted over time and as the experimental protocols evolved. Our experimental paradigm followed an approach we have termed continuous FAIRness (47), in which data associated with an investigation is findable, accessible, interoperable, and reusable (48) through the data life cycle. As part of this approach, every figure in the paper was assigned a globally unique DOI that links to all the relevant primary data and any intermediate data products. We also carefully captured details of experimental protocols including sequences of all plasmid constructs, microscope configuration parameters, and exact versions of all software used for analysis. By storing this information and any additional metadata at every step of our experiments, we can significantly reduce the potential for errors in data entry, analysis, or interpretation. Finally, all readers can easily access the raw data and the detailed information about experimental and analytical methods, which will enable others to reproduce our results.

Neuronal Activation in the Pallium Changes with Memory Formation. Because the amygdala is the central locus of FC in mammals and the dorsal pallium of teleost fish is thought to contain the homolog of the amygdala, we reasoned that functional changes were likely to occur in pallial neurons following TFC. To identify such areas, we examined regional differences in the expression of pERK (phosphorylated extracellular signal-regulated kinase), a marker for neuronal activity (49), in response to the CS in 14 to 16 dpf L and NL fish. L fish showed marked enrichment in pERK in a discrete, anterolateral region in the pallium following presentation of the CS (Fig. 2*A* and *SI Appendix*, Fig. S2*A*). This

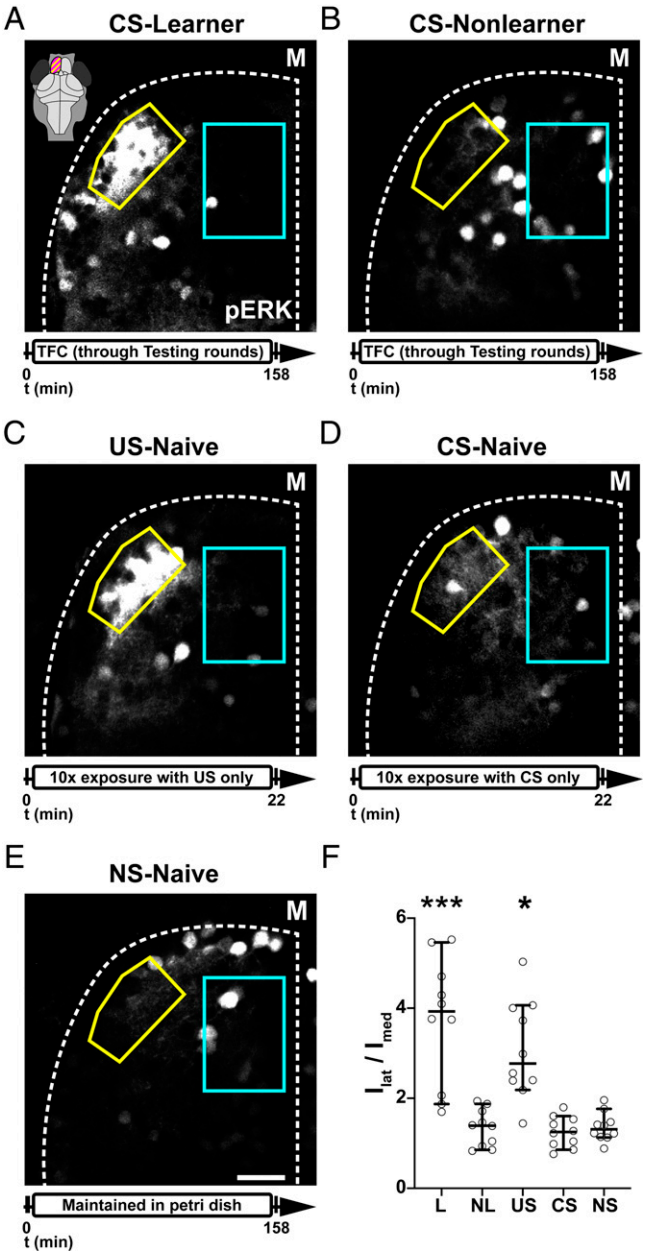

Fig. 2. Neuronal activation within the anterolateral pallium in response to the CS in learner fish and to the US in naïve fish. (*A*) Intense immunostaining of pERK in the pallium (magenta highlighted region, *Inset*) of an L fish exposed to 5 CSs following TFC. The strong signal in an anterolateral region (yellow outline) of this optical section reveals regional neuronal activation. Relatively less immunostaining is present in the medial pallium (cyan outline). (*B*) An NL fish shows a lack of pERK staining in the anterolateral region (yellow outline) after exposure to 5 CSs in this equivalent optical section. (*C*) A naïve fish reveals strong pERK staining in the same anterolateral region (yellow outline) after exposure to 10 USs. Equivalent optical section to those in *A* and *B*. (*D*) A naïve fish exposed to 10 CSs does not show concentrated pERK labeling in the anterolateral region (yellow outline). Optical section equivalent to those in *A*–*C*. (*E*) A naïve fish not exposed to a CS or US (NS) does not show concentrated pERK labeling in the anterolateral region (yellow outline). Optical section equivalent to those in *A*–*D*. (*F*) L and US-exposed naïve subjects show a significantly higher lateral:medial pERK intensity ratio compared to NL and naïve untreated subjects (*$P < 0.02$, ***$P < 0.005$, $n = 5$ fish per group, Kruskal–Wallis multiple comparison test). White dashed lines mark the border of the pallium (midline = M) in *A*–*E*. (Scale bar for *A*–*E*, 20 μm.) Data available at https://doi.org/10.25551/1/1-1JP0 (50).

enrichment was absent in NL fish under similar conditions, indicating that the pERK labeling was not simply a response to the US the fish were exposed to during TFC (Fig. 2*B* and *SI Appendix*, Fig. S2*B*). To further characterize pallial function, we exposed naïve fish to repeated presentations of the US (see Materials and Methods). We found elevated pERK in a discrete region in the anterolateral pallium that colocalized with the CS-responsive region identified in the L fish (Fig. 2*C*, yellow outline, and *SI Appendix*, Fig. S2*C*). Naïve fish exposed only to the CS or fish not exposed to either the CS or US showed relatively little staining in the anterolateral pallium (Fig. 2 *D* and *E* and *SI Appendix*, Fig. S2 *D* and *E*). Thus, the activity marker response in the pallium to the CS in L fish looked similar to that from the US in naïve fish, consistent with the CS activating the same population of neurons after learning as the US activates in naïve fish.

We quantified these responses by taking the ratio of total pERK labeling within the anterolateral region divided by the total pERK labeling in the medial region (I_{lat}/I_{med}). In response to the CS, I_{lat}/I_{med} in L fish was significantly higher than in NL fish, CS-exposed, and -unexposed naïve fish. Exposure to the US in naïve animals also significantly increased I_{lat}/I_{med} compared to NL and CS-exposed and -unexposed naïve animals (Fig. 2*F*; $P < 0.005$ and $P < 0.05$, respectively; Kruskal–Wallis test). L fish exposed to the CS and naïve fish exposed to the US revealed similar I_{lat}/I_{med} (Fig. 2*F*; $P > 0.05$, Kruskal–Wallis test). Thus, our results suggest that following learning, cells that respond to an aversive stimulus in naïve fish become responsive to the CS with which the aversive stimulus is associated.

Labeling Excitatory Synapses in Live Fish. Having established that TFC can lead to memory formation and a change in the pattern of activity in the pallium of larval zebrafish, we sought to examine how it affected the distribution of pallial synapses. Accordingly, we visualized excitatory synapses within the pallium using PSD-95.FingR, a recombinant probe that binds with high affinity and specificity to PSD-95, a major postsynaptic component of excitatory synapses (51) and a marker for synaptic strength (52–54). PSD-95.FingR labels postsynaptic sites without causing structural or functional changes in mammalian neurons (55). PSD-95.FingR also labels synapses in living zebrafish larvae (56). To produce neuronal labeling that is sufficiently sparse to resolve individual synapses within the dense neuropil region of the pallium, we induced mosaic transgenic expression of PSD-95.FingR by coinjecting linearized plasmid DNA encoding the FingR reporter with transposase messenger RNA (see Materials and Methods) into zebrafish zygotes (Casper background) (57). Such mosaics, coexpressing PSD-95.FingR-GFP and membrane-targeted mScarlet, show the expected spine-like protrusions on dendrites, with GFP labeling at the tips, consistent with PSD-95.FingR labeling excitatory synapses (Fig. 3*A*; pallial neurons imaged in 14 to 16 dpf zebrafish, 4.0 to 5.0 mm SL). Furthermore, PSD-95.FingR labeling intensity at individual puncta was proportional to mScarlet labeling intensity at colocalized spine heads ($R = 0.68$), a measure of spine-head size (Fig. 3*A*). Finally, exogenous PSD-95-RFP and PSD-95.FingR-GFP colabeled discrete puncta at proportional levels (*SI Appendix*, Fig. S3, $R = 0.9$), consistent with PSD-95 FingR labeling PSD-95 in a stoichiometric manner. Accordingly, we will refer to puncta labeled with PSD-95.FingR-GFP as synapses. Note that nuclei of the expressing cells are labeled due to the transcriptional regulation system, which targets excess, unbound protein to the nucleus ("N" in Fig. 3*A*) and inhibits transcription (55). FingR transgenic fish did not display any difference in the FR versus wild-type fish, suggesting that the presence of the transgene does not diminish learning ability ($P > 0.05$, Mann–Whitney *U* test; *SI Appendix*, Fig. S3).

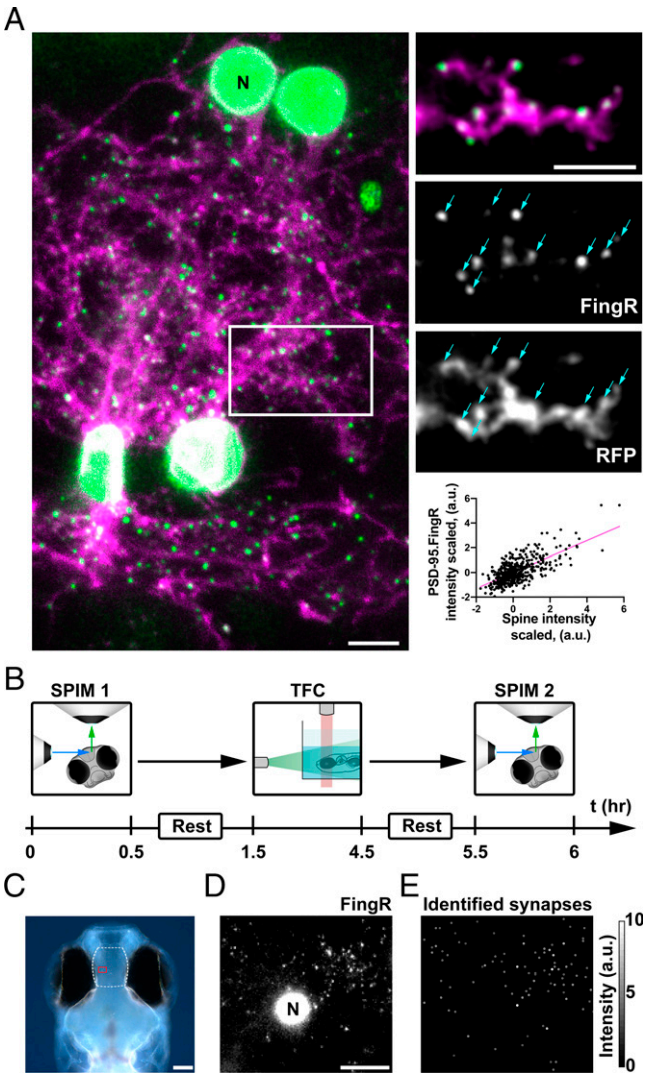

Fig. 3. Imaging excitatory synapses in larval zebrafish. (*A*) Confocal image of neurons coexpressing PSD-95.FingR-GFP (green) and membrane-targeted mScarlet (magenta) in the pallium of a living 14 dpf zebrafish larva. Subset maximum intensity projection of the boxed region is to the right. (*Top Right*) PSD-95.FingR-GFP puncta colocalize with the tips of spine-like projections. (*Middle*) PSD-95.FingR-GFP. (*Bottom*) mScarlet ("RFP"). Arrows point to spine-like projections that colocalize with PSD-95.FingR-GFP puncta. (*Bottom Right*) Intensities of PSD-95.FingR labeling at individual puncta were roughly proportional to intensities of mScarlet labeling at the same puncta; for cells shown at left, $R = 0.68$). (*B*) Schematic of TFC/SPIM imaging experiments. The zebrafish is rotated by $\theta = 25°$ from the fluorescence detection axis (green arrow) to avoid illuminating the eyes with the incident light sheet (blue arrow). (*C*) Dorsal view of a 15 dpf larval zebrafish head with pallium region imaged by SPIM outlined with dashed white line. (*D*) Maximum intensity projection of a stack of SPIM images of PSD-95.FingR (red outlined region in *C*) showing synaptic puncta and a bright nucleus (N). (*E*) Map of synapses identified from *D* (see Materials and Methods). Gray scale intensity reflects total PSD-95.FingR labeling for each punctum. (Scale bar in *A*, 5 μm; *C*, 100 μm; *D* and *E*, 10 μm.) Data available at https://doi.org/10.25551/1/1-1JP2 (58).

Total Synapse Number in the Pallium Does Not Change following TFC. To interrogate how learning affects synapses in the pallium, we imaged PSD-95.FingR-GFP fish before and after the animals underwent TFC using SPIM (Fig. 3 *B* and *C*). The stoichiometric relationship between PSD-95.FingR-GFP and endogenous PSD-95 protein (55) resulted in relatively dim synapse labeling, presenting a significant challenge for live imaging. We customized our SPIM for zebrafish larvae imaging (*SI Appendix*, *SI Methods*) to

provide high contrast and speed necessary to image labeled synapses while minimizing laser-induced toxicity, which is essential to maintain TFC learning capability in imaged animals. These customizations allowed us to acquire three-dimensional (3D) images of fish brains with an optical resolution of ~0.5 μm laterally and 1.3 microns axially (*SI Appendix*, Fig. S4*A*).

We identified synapses in the left pallium from volumetric images in a two-step process mediated by the data management system (see Materials and Methods). A custom computer program identifies 3D intensity maxima in denoised (low-pass filtered) image stacks (*SI Appendix*, Fig. S4 *B–D*), and then blinded segmenters confirm or reject these putative synapses. This approach generates a 3D map of positions and intensities of PSD-95.FingR puncta, corresponding to excitatory synapses (Fig. 3 *D* and *E*). We imaged an average of 1,155 synapses per fish, roughly 0.5% of the total synapses in that region (see Materials and Methods, *SI Appendix*, Fig. S4 *E* and *F*). When the total number of synapses before versus after TFC was compared for L, PL, and controls (CS only, US only, and NS) over the entire pallium, no significant difference was found. A modest decrease (~10%) was found for NL (Fig. 4*A*; $P > 0.05$ for L, PL, and controls; $P < 0.05$ for NL, Wilcoxon test). Additionally, synapse numbers did not differ significantly between L, NL, PL, and control fish at either time point (*SI Appendix*, Fig. S5; $P > 0.05$, Kruskal–Wallis test). Thus, our data indicate that TFC learning is not associated with a significant change in the total number of synapses in the pallium. To compare distributions of synapses, we aligned SPIM images from the same fish at two time points (before and after TFC) using a rigid body transformation that optimizes overlap of labeled nuclei (see Materials and Methods and Fig. 4*B*). We identified synapses that became undetectable (lost synapses) or detectable (gained synapses) following TFC by uniquely pairing each synapse from the before-TFC image with the synapse closest to its position in the after-TFC image (Fig. 4*C*). Unpaired synapses from the before-TFC image (more than 4 μm from a potential counterpart in the after-TFC image) were designated as lost synapses; unpaired synapses from the after-TFC image (without a counterpart <4 μm away in the before-TFC image) were considered gained synapses (see Materials and Methods and Fig. 4*D*). The 4-μm standard is based on comparisons of aligned 3D images of the same Dendra-labeled neuron taken 5 h apart, which corresponds to the time required for TFC with rest periods. The vast majority of spine tips visible at both time points moved less than 4 μm (*SI Appendix*, Fig. S6). Categorizing and tallying synapses in this manner revealed that the overall rate of synapse loss or formation and the fraction of synapses present at both time points did not vary significantly between L, PL, NL, and control fish (Fig. 4 *E–G*; $P > 0.05$, Kruskal–Wallis test). When we measured synapse gain and loss from the Dendra-labeled pallial neurons imaged 5 h apart for four fish, the rates obtained were similar to those calculated using images of PSD-95.FingR-labeled neurons (*SI Appendix*, Fig. S6).

Region-Specific Synapse Gain and Loss in Learners. To discern spatial patterns of synaptic change for each group of fish, we coaligned the synaptic datasets onto a single template zebrafish brain (see Materials and Methods and *SI Appendix*, Fig. S7) and combined them to create cumulative distributions (CDs) of lost and gained synapses (Fig. 5*A*). In L fish, the CD showed a concentration of gained synapses in the lateral versus medial pallium (Fig. 5*A*). To quantify and statistically evaluate this potential regional disparity, we used a support vector machine algorithm to define a decision boundary plane (DB plane, see Materials and Methods) that optimally divides the synapse map into two regions: one in which synapses gained minus lost is maximized and one in which it is minimized. The DB plane sharply divides the cumulative distribution of synapses from learners into a region of overall synapse gain and one of synapse loss. In contrast, synapse loss and

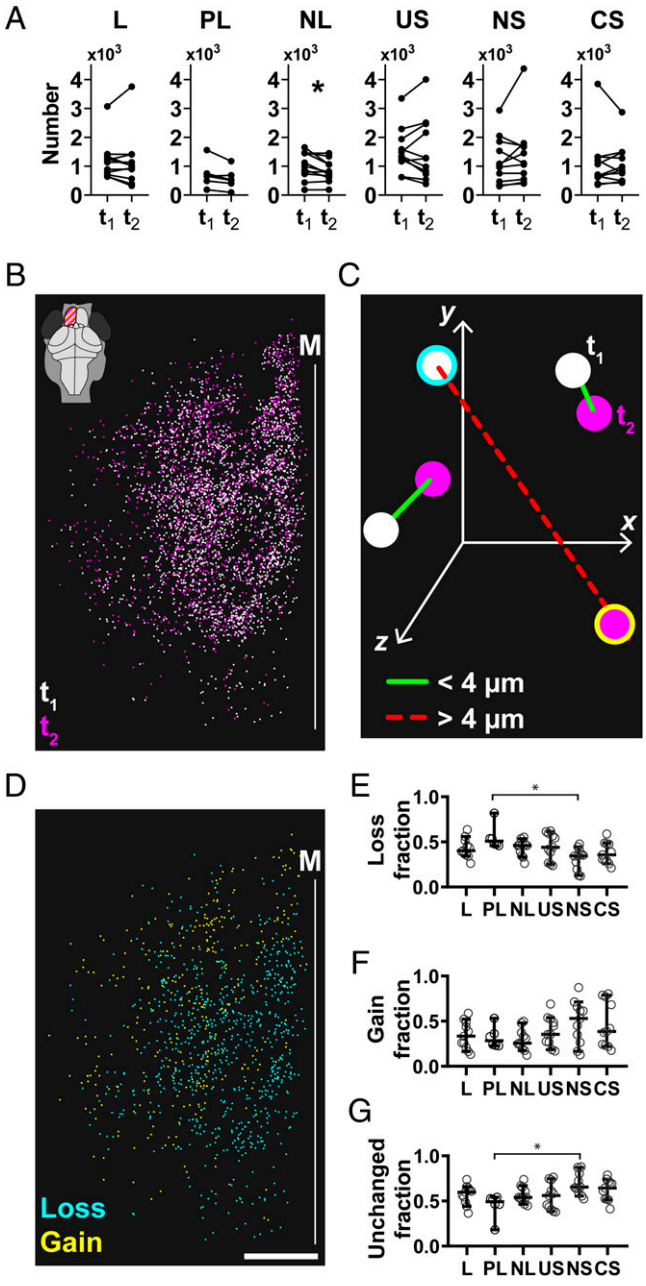

Fig. 4. Synapse changes with TFC in larval zebrafish. (*A*) Total number of synapses before (t_1) and after (t_2) TFC for individual fish ($P > 0.05$ for L, PL, US, NS, and CS; $^*P < 0.05$ for NL, Wilcoxon test). (*B*) Dorsal view of all identified excitatory synapses in the left pallium (highlighted in inset) of a learner fish before (white) and after (magenta) TFC alignment of the two synapse images was accomplished by manually identifying and then computationally aligning the labeled nuclei (not shown in images). (*C*) Schematic of algorithm to identify synapses lost or gained following TFC. All synapses were grouped into pairs, one from before TFC and the second from after, such that the distance between the pair is minimized. Each synapse could only be part of a single pair. All pairs separated by a distance greater than or equal to 4 μm are considered different synapses (i.e., lost if from before TFC or gained if from after). (*D*) Dorsal view of lost (cyan) and gained (yellow) synapses following TFC from the learner fish shown in *B* reveals more lost synapses medially and more gained synapses laterally. (*E–G*) Synapse turnover in fish before and after TFC did not show significant variation between different categories of fish ($P > 0.05$, Kruskal–Wallis test) except for PL and NS (loss fraction and unchanged fraction, $P < 0.05$, Dunn's multiple comparison test). (Scale bars, 20 μm.) $n = 11$ L, 6 PL, 11 NL, 11 US, 11 NS, and 11 CS fish. Data available at: https://doi.org/10.25551/1/1-1Z04 (59).

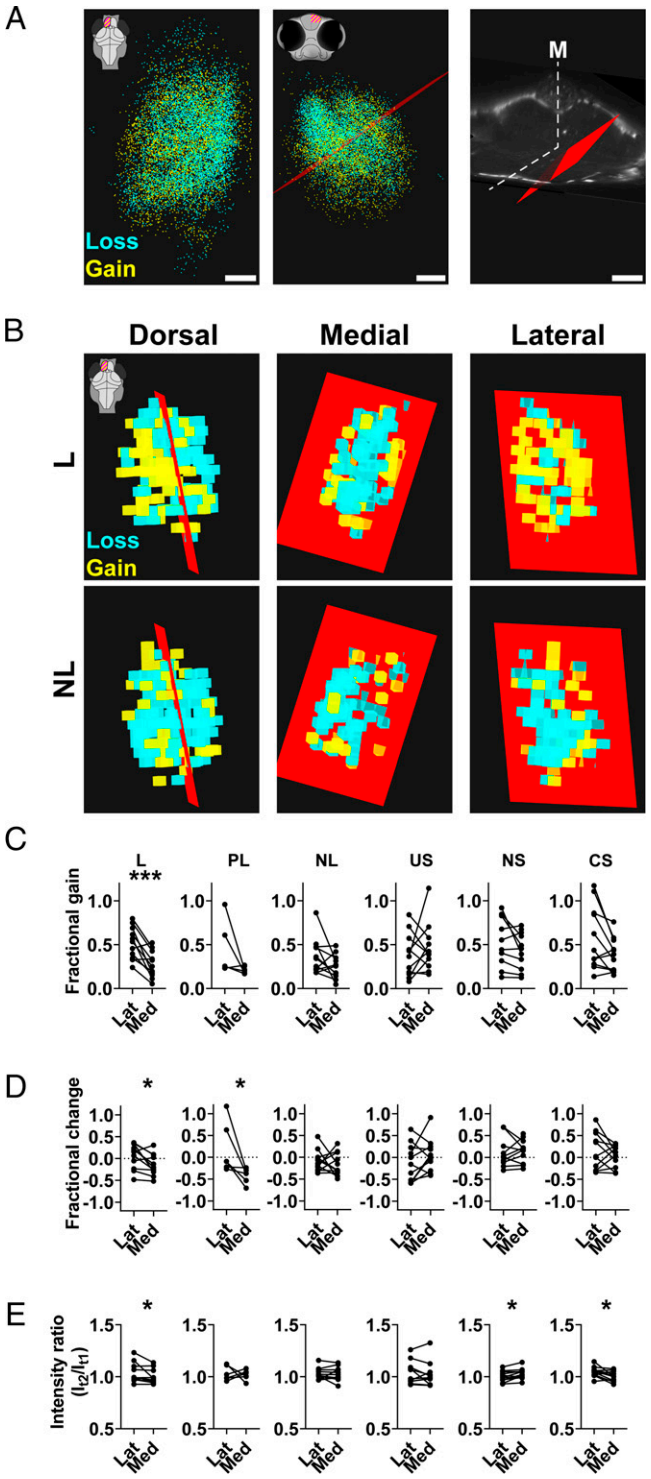

Fig. 5. Regional differences in synapse formation in the pallium of learner fish. (*A*, *Left*) Map of lost (cyan) or gained (yellow) synapses in the left pallium following TFC for L fish in dorsal view (highlighted in inset, midline to the right). Results from each fish were registered onto a canonical fish prior to pooling (*SI Appendix*, Fig. S7). (*Middle*) Coronal view of pooled L results shows a DB plane (red) that optimally divides the left pallium into two regions of differential synapse change: dorsomedially, synapse loss predominates; ventrolaterally, synapse gain predominates (region highlighted in inset; midline to the left). (*Right*) Slightly tilted 3D coronal view of DB plane for L fish (red) shown against the outline of the canonical zebrafish brain (gray; M: midplane). (*B*) Dorsal (highlighted in inset cartoon, medial to the right), medial, and lateral views of voxelized aggregate synaptic data in L and NL fish. Each voxel represents a region with predominant synapse loss (cyan) or gain (yellow) following TFC. The DB plane (red) derived from L separates a region of predominant synapse gain (ventrolaterally) and loss (dorsomedially) in L; the same plane does not separate loss and gain in NL. (*C*) Synapse fractional gain analysis for each group reveals that learners have gained significantly more (~30%) synapses ventrolaterally versus dorsomedially relative to the DB plane (***$P < 0.005$, Wilcoxon test). PL, NL, and control groups do not show a significant difference in synapse gain between the two sides of the DB plane ($P > 0.05$, Wilcoxon test). (*D*) Fractional change in synapses (gained minus lost) is significantly higher ventrolaterally versus dorsomedially in L and PL (*$P < 0.05$, Wilcoxon test) but not in any other groups ($P > 0.05$, Wilcoxon test). (*E*) The ratio of PSD-95.FingR-GFP fluorescence intensity per synapse before and after TFC (I_{t2}/I_{t1}) is negligibly different in medial versus lateral regions in L (~1% difference), CS, and NS (≤5% difference, *$P < 0.05$, Wilcoxon test), and in US, PL, and NL (<4%, $P > 0.05$, Wilcoxon test). (Scale bar, 20 μm.) Voxel dimensions in *B*, 10 μm. $n = 11$ L, 6 PL, 11 NL, 11 US, 11 NS, and 11 CS fish. Data available at https://doi.org/10.25551/1/1-1Z06 (60).

gain were distributed randomly throughout the pallia of NL and control fish (Fig. 5*B* and *SI Appendix*, Fig. S8*B*). PL fish show an intermediate result, with increased synapse gain in the ventrolateral area and loss in the dorsomedial area but with a less dramatic difference than observed in L fish (*SI Appendix*, Fig. S8*B*).

Using a modification of the leave-one-out test, we assessed whether the pallia from fish of a particular type could be divided into regions with statistically different rates of synapse gain and/or loss (see Materials and Methods). For each group of fish, we calculated a cumulative distribution of synapses from all fish except one as a training dataset to determine the DB plane based on gained minus lost synapses. We then used this group-minus-one DB plane to define the ventrolateral and dorsomedial areas in the excluded fish and determine the total number of lost or gained synapses associated with those regions. In L fish, the median fractional synapse gain was ~30% higher on the ventrolateral side of the pallium versus the dorsomedial side, reflecting a significant interregional disparity (Fig. 5*C* and *SI Appendix*, Fig. S8*A*; $P < 0.005$, $n = 11$, Wilcoxon test). No significant interregional disparities in synapse gain were found for NL, CS, US, or NS fish (Fig. 5*C*; $P > 0.05$, $n = 11$, Wilcoxon test) or for PL fish ($P > 0.05$, $n = 6$, Wilcoxon test), and the magnitudes of the median differences were less than 11%. L, PL, NL, and CS fish had no significant dorsomedial versus ventrolateral disparities in synapse loss (*SI Appendix*, Fig. S8; $P > 0.05$, Wilcoxon test) with median magnitudes <13% for L, NL, and CS and <21% for PL. In contrast, small (<12%) but significant increases in medial versus lateral synapse loss were seen in US and NS fish (*SI Appendix*, Fig. S8 *B* and *C*; $P < 0.05$ and $P < 0.005$, respectively; Wilcoxon test). Synapse change (gained minus lost synapses) was higher in the ventrolateral area than in the dorsomedial area of L and PL fish ($P < 0.05$, Wilcoxon test; Fig. 5*D*), with median differences >25%. No significant synapse change was seen between dorsomedial and ventrolateral regions of NL or control fish (Fig. 5*D*; $P > 0.05$, Wilcoxon test), and median differences were <10% for CS, NS, and NL and <25% for US.

To assess synapse change associated with learning using raw SPIM images, we examined PSD-95.FingR labeling in corresponding lateral and medial regions captured before and after TFC in an L and NL fish taken from the fully analyzed cohort. In L fish, the lateral area showed a greater increase in gained synapses after TFC than the medial area, whereas the number of gained synapses in each region was comparable in NL fish (*SI Appendix*, Fig. S9), corroborating our DB-plane findings.

Intensity of Synaptic Labeling Does Not Change Systematically with Learning. Having aligned synaptic distributions allows us to further characterize changes in synapses, by testing whether we can detect a significant change in fluorescent PSD-95.FingR-GFP labeling. The median value measured for PSD-95.FingR-GFP labeling of synapses before and after TFC was not significantly

different for any of the different groups (*SI Appendix*, Fig. S10*A*; $P > 0.05$, Wilcoxon test). We also performed regional analyses of PSD-95.FingR-GFP labeling changes in the pallium following TFC to reveal possible spatial patterns of differential change in synaptic strength. Based on the ratio of the intensity of PSD-95. FingR-GFP labeling before and after TFC for each synapse present at both time points (I_{t2}/I_{t1}), DB planes were determined that divided regions of maximal I_{t2}/I_{t1} from regions of minimal I_{t2}/I_{t1} for each fish using the leave-one-out method, as with gained and lost synapses (see Materials and Methods). The median difference in I_{t2}/I_{t1} between the ventrolateral and dorsomedial regions was ∼1% of the median intensity of labeling for L fish and ≤5% for all other groups (Fig. 5*E*). Furthermore, distributions of I_{t2}/I_{t1} for the two regions on either side of the DB planes for L, PL, NL, and controls are very similar (*SI Appendix*, Fig. S10). These results suggest that memory formation did not cause a systematic change in the labeling of synapses detected before and after TFC.

It might be argued that there was indeed systematic change in synaptic strength due to memory formation in our imaged fish but that the strength increases or decreases reflected in the fluorescence intensity happened in a way that moved dim synapses below or above the detection threshold, which then were interpreted by our analysis as lost or gained synapses. To test this, we examined the distribution of intensities of lost, gained, and unchanged synapses. If synapses simply moved above or below the detection threshold as a result of a small gain or loss in intensity, we would expect that the distribution of intensities of lost synapses (at t_1) and those of gained synapses (at t_2) would be clustered at low intensities relative to the distributions of unchanged synapses. However, the distributions of lost and gained synapses are very similar to those of unchanged synapses (*SI Appendix*, Fig. S11). A total of 47% of lost synapses and 44% of gained synapses have intensities higher than the median intensity for all synapses at t_1 and t_2 respectively; 11% of lost synapses and 10% of gained synapses are among the brightest 15% of all synapses at t_1 and t_2, respectively. Thus, it is very unlikely we are mistakenly interpreting dim synapses that underwent modest intensity loss or gain as lost or gained synapses. As an additional test of this potential artifact, we simulated the effects of reducing the intensity of synapse labeling by different percentages and then determined which synapses would have intensities below the detection threshold and thus be considered lost. After calculating the resulting intensity distributions (at t_1) corresponding to simulated lost synapses, we found that a dramatic intensity loss (∼80%) is required to produce a distribution of lost synapse intensities similar to the distribution obtained from experimental data (*SI Appendix*, Fig. S11*G*). Comparable results were found for gained synapses (*SI Appendix*, Fig. S11*I*). To further test the sensitivity of our analysis to fluctuations in intensity, we reduced the intensity of a synaptic image stack for a particular fish by 10% while keeping the same noise level and resegmented the synapses in the new stack. Comparison of images before and after this manipulation showed that >98% of the original synapses were present in both images, suggesting that our analysis is relatively impervious to small fluctuations in intensity (*SI Appendix*, Fig. S11*J*). Thus, synapses referred to as gained or lost likely represent synapses that appeared, disappeared, or underwent a dramatic increase or decrease in PSD-95. FingR labeling.

Synapse Gain within the Anterolateral Pallium. To investigate whether changes in synaptic structure are related to alterations in neuronal function, we examined the correlation between regions in which synapse change occurs during memory formation and regions of intense cellular activity during memory formation and retrieval as assayed by pERK (Fig. 2). Our results show a distinct anterolateral region of neuronal activation labeled by pERK in response to the US in naïve fish and the CS in learner fish (Fig. 2 *A* and *C*). This region aligns with the region on the ventrolateral side of the DB plane corresponding to synapse gain in learner fish after TFC (Fig. 6*A*). However, because pERK labeling is primarily in cell bodies and synapses are primarily on dendrites, we sought to compare the locations of dendrites from cells with cell bodies within the anterolateral region of activation to the region in which we saw synapse gain in L fish (Fig. 6*A*). To visualize dendrites of individual cells in vivo, we expressed the photoconvertible protein Dendra in fish brains and then photoconverted isolated pallial cells using primed conversion (61). Mapping the full extent of the processes of five neurons with somata within the anterolateral pallial region revealed that they are predominantly (∼90%) contained within the region of increased synapse formation (Fig. 6*B*). We also compared the synapse gain in a region of the pallium defined by the processes of these anterolateral cells with an area similarly defined by processes of cells within the medial region in Fig. 2 (Fig. 6*C*) and found that there were significantly more gained synapses in the lateral than in the medial cells in L and PL ($P < 0.005$ and $P < 0.05$, respectively; Wilcoxon test; Fig. 6*D*). In contrast, in NL and control fish, the number of gained synapses in the two areas was not significantly different ($P > 0.05$, Wilcoxon test; Fig. 6*D* and *SI Appendix*, Fig. S12). Synapse change in the two regions was also significantly different in L and PL ($P < 0.05$, Wilcoxon test) but not in NL or controls ($P > 0.05$, Wilcoxon test; Fig. 6*E* and *SI Appendix*, Fig. S12). There were no significant differences in the relative number of lost synapses in the two areas for fish in any of the experimental groups ($P > 0.05$, Wilcoxon test; *SI Appendix*, Fig. S12). Thus, regions of synapse gain in the lateral pallium following memory formation overlap with regions containing neurons that are active during memory formation and retrieval.

Finally, photoconversion labeling experiments revealed that a subset of cells in the anterolateral pallial region send their projections ventrally and posteriorly through the subpallium, suggesting they are output neurons (*SI Appendix*, Fig. S13). Our results are consistent with the anterolateral region of the pallium containing cells that respond to aversive stimuli in naïve fish, which, after TFC, are activated by the neutral stimulus following concentrated generation of new excitatory synapses.

Discussion

We have developed a paradigm for mapping changes in the distributions of synapses in the brains of living larval zebrafish over time using longitudinal imaging. Our results show that following associative memory formation in response to CC, significant region-specific changes in the rate of synapse formation occur. More synapses formed in the ventrolateral region of the pallium relative to the dorsomedial region following CC in learner fish (both Ls and PLs) but not in NL and control fish. Even with this regional change, the total number of pallial synapses in all fish did not change significantly. Surprisingly, we detected only small total or region-specific average changes in the labeling intensity of PSD-95 at synapses present before and after learning.

Previous studies using post hoc labeling have found that hippocampal engram cells have increased spine density relative to nonengram neurons following contextual fear conditioning (CFC) in mice (17, 28, 63). Although these studies did not directly measure synapse change, their results are nonetheless consistent with our conclusion that memory formation is associated with region- and cell-specific increases in synapse formation. This interpretation is also consistent with recent work showing that selectivity of neurons in the ferret visual cortex arises from the most common visual inputs rather than from the strongest inputs (64). In contrast, our observation that long-term PSD-95.FingR labeling of synapses changed minimally with learning, even in

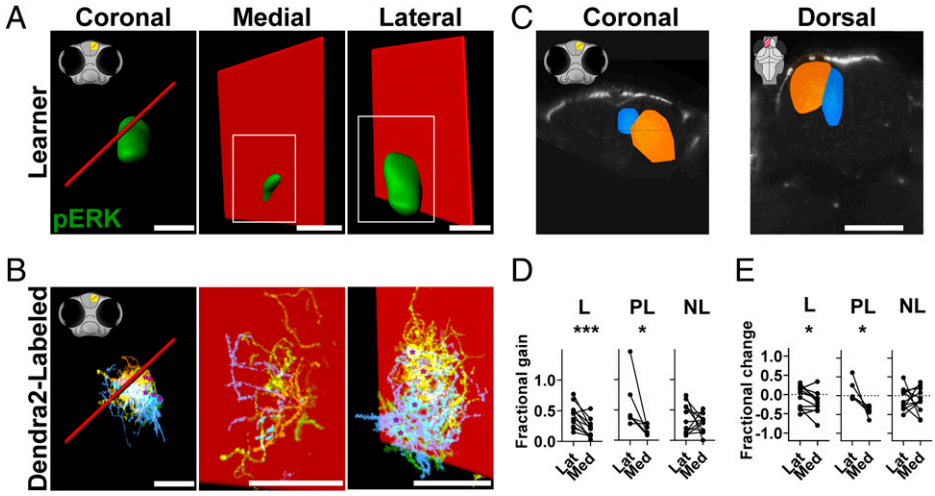

Fig. 6. Anatomical correlation of regions of increased neuronal activity and synaptic gain following TFC. (*A*) Coronal (*Left*), dorsomedial (*Middle*), and ventrolateral (*Right*) views of the region of increased pERK labeling in the left pallium of learner fish (see inset cartoon) exposed to CS. pERK staining is located mainly on the ventrolateral side of the DB plane, where synapse gain predominates in learners. (*B*) Five individually photoconverted cells (see Materials and Methods), whose cell bodies lie within the pERK staining area of the pallium shown in *A*, have processes that are predominantly (~90%) on the ventrolateral side of the DB plane. Coronal (*Left*), dorsomedial (*Middle*), and ventrolateral (*Right*) views. Magenta asterisks in left and right subpanels indicate the position of cell bodies. (*C*) Volumes defined by the dendrites of medial (blue) and anterolateral (orange) cells, corresponding to regions outlined in cyan and yellow, respectively, in Fig. 2 *A*–*E*. (*D*) Fractional synapse gain is significantly higher for L (***$P < 0.005$, Wilcoxon test) and PL (*$P < 0.05$, Wilcoxon test) in the anterolateral region than in the dorsomedial region but not in NL. (*E*) Fractional synapse change (gained synapses minus lost synapses) is also significantly higher in L and PL (*$P < 0.05$, Wilcoxon test) but not in NL. (Scale bars in *A* and *B*, 30 μm. Scale bar in *C*, 100 μm.) Data available at https://doi.org/10.25551/1/1-1Z08 (62).

regions in which dramatic gain and loss of synapses occurred, would appear to be at odds with previous studies. In particular, a recent imaging study found that spines on CA1 engram cells have approximately twice the volume of spines in nonengram cells following CFC (28). This apparent discrepancy could be explained by several differences between our study and previous ones. Specifically, earlier studies depended on post hoc comparisons of synapses on different cells, whereas we directly compare the same synapses at two separate time points. In addition, the memories studied here were formed in the brains of a different species (fish versus mice), at a different age (larvae versus adults), in a different brain region (pallium versus hippocampus), in a different cell type (pallial neurons versus CA1 neurons), and as a result of a different learning paradigm (TFC versus CFC) compared with previous studies. Furthermore, increases in synaptic strength could have occurred in a subset of sparsely distributed pallial cells, causing these increases to be obscured by noise. They could also have been transient and disappeared prior to the second imaging. In addition, synaptic strength could have changed as a result of presynaptic mechanisms our paradigm could have missed. Finally, nonsynaptic changes that would have been difficult to detect with our system, such as increases in neuronal excitability or myelination, could have contributed to learning (65, 66).

Our detection and analysis methods do not permit gold-standard validation of synapses, such as can be obtained with electron microscopy. Thus, our conclusions rest on the assumption that our methods, validated by correlative and suggestive evidence, accurately identify excitatory synapses. In addition, although PSD-95 is a well-established marker for synaptic strength, particularly in mammalian systems (53), we cannot rule out the possibility that there are instances in which changes in levels of PSD-95 do not reflect changes in synaptic strength.

Our results with pERK labeling showed that cells within a discrete region in the anterolateral pallium respond intensely to both the US in naïve fish and the CS in learner fish. This anterolateral region is thus active both during memory formation and retrieval (67, 68). Importantly, this region overlaps with the area in which intense synapse formation occurs in learners. Our pERK results corroborate those of a recent study in which Ca^{2+} activity in the mouse amygdala imaged before and after FC showed that the pattern of cellular responses to the CS following learning became similar to responses to the US in naïve mice (69). These anterolateral pallial cells may be homologous to aversive cells found in the basolateral amygdala in mice (27, 70). However, unlike aversive amygdalar cells in the mouse, which are distributed in a salt-and-pepper pattern, those in the anterolateral pallium appear to be tightly clustered, making them easier to visualize and suggesting that they might be amenable to investigations into how neurons encode fear.

Our findings demonstrate the power of integrating reproducibility and transparency into all stages of a scientific investigation, benefiting both the researcher and the broader research community (71). A scientific environment that ensured that all data were FAIR throughout the life cycle of the investigation was made possible by designing experiments and analysis around a data management platform that is easily customized as experiments evolve (48, 72). We suggest such scalable and modular data management strategies become standard for data collection and presentation in the scientific community. The tools presented here provide a foundation for such efforts, since few alternatives exist in the literature that stress FAIR principles (73).

This study combines informatics, imaging, and molecular neuroscience to perform unbiased spatial mapping of learning within intact brains over time at the scale of individual synapses. Thus, our approach provides a needed link between classical studies of learning and more fine-grained analyses. The results provide fundamental insight into how the microstructure of the brain can change physically to encode information and offers a unique perspective from which to study the relationship between brain structure and function.

Materials and Methods

TFC. TFC is a cued CC paradigm that causes the fish to associate a CS consisting of a green light with a US consisting of heating from a near-infrared (NIR) laser. Tail flicking comprises the UR in the naïve fish and the CR in the learner fish. All behavioral experiments were performed on a custom-built TFC scope that enables the presentation of stimuli to be correlated with tail-flick behavior (*SI Appendix*, Fig. S1*B*).

SPIM. A previously reported custom-built SPIM (74) was used for live-imaging experiments related to the TFC protocol. Briefly, light from a 488-nm laser is focused at the sample using a low numerical aperture (NA) illumination objective and scanned (1 kHz) by a galvanometer mirror to create a light sheet. The scanned light sheet was positioned at the focus of the detection objective by a second galvanometer mirror to enable optical sectioning. Sample fluorescence generated by the excitation light sheet is captured by a high-NA objective. The emission path is perpendicular to the excitation path; both the excitation and emission paths are parallel to the plane of the support air table. The fluorescence signal passes through a tube lens and a spectral image splitter to enable simultaneous acquisition of green GFP fluorescence, as well as red tissue autofluorescence, on the same scientific complementary metal-oxide semiconductor (CMOS) camera.

Data Management. The data management system used in this work, which stores and processes raw data and analysis results, is based on a custom Deriva data management platform developed in house (72). This includes digital asset storage for microscopy data and other ancillary data files, with a rich metadata catalog to track assets and their scientific context. Robust data management practices help to maintain clear data provenance records and accommodate additions/changes to experimental methods over time.

Analysis of Behavioral Data. The result of an experiment on the TFC scope (Fig. 1 *A–D* and *SI Appendix*, Fig. S1 *C–E*) is a top-down fixed-perspective time-lapse movie of the entire body of a subject (14 to 16 dpf zebrafish larva). The dorsal view places the larva roughly along the horizontal midline of the imaging frame, with the head fixed to the left and the tail free to move in the right half of the frame. Stages of the experimental protocol (when the CS and US turn on or off) are signaled in band by abrupt changes in global infrared illumination (by the wide-field NIR illumination LED), which are apparent to the camera but invisible to the subject. Behavioral analysis is a multistage process computed from this movie (*SI Appendix, SI Methods*).

Synapse Detection in Images. During in vivo SPIM imaging, anisotropic open microscopy environment tagged image file format (OME-TIFF) volumes are recorded with spatial sampling of 0.26 × 0.26 microns in plane and 0.4-μm steps between planes. A region of interest is manually identified by an experimentalist for the two time-point images of each zebrafish larva. Within each region of interest, a two-stage synapse detection process proceeds: an algorithm performs an automated scale-sensitive local peak detection to identify candidate synapses and a human operator classifies points as synapses by reviewing each candidate (*SI Appendix*, Fig. S4 *B–D*) within a bespoke, interactive classification tool developed in house. The detected synapses of one region are saved in a tabular comma-separated values (CSV) file containing centroid voxel coordinates and local image measurements (synapse intensity within a 3D volume around the centroid) for each synaptic point.

Statistical Analysis. Statistics (nonparametric pairwise and nonparametric ANOVA analyses) were calculated using Prism 8 (Graphpad Software, LLC). Nonparametric tests were applied, since the data could not be assumed to be normally distributed. No statistical methods were used to predetermine sample size.

Data Availability. All raw and processed data from this study were created following FAIR data principles and are available in the public Data Repository at the University of Southern California known as Synapse (https://synapse.isrd.isi.edu) (75). Data is also available at https://doi.org/10.25551/1/1-1YZE, https://doi.org/10.25551/1/1-1JP0, https://doi.org/10.25551/1/1-1JP2, https://doi.org/10.25551/1/1-1Z04, https://doi.org/10.25551/1/1-1Z06, and https://doi.org/10.25551/1/1-1Z08. All other study data are included in the article and/or *SI Appendix*.

ACKNOWLEDGMENTS. We thank M. Jones and C. Arnesano for microscopy technical support in the Translational Imaging Center and L. Trinh and E. Carranza Lopez for zebrafish husbandry support. We thank M. D'Arcy for bespoke software development and all members of the Informatics Systems Research Division at the University of Southern California Information Sciences Institute for contributions to the data management system. We thank K. Watanabe, H. Jin, E. Yang, L. Oganessian, P. Richards, N. Karimi-Mostowfi, W. Liu, Y. Davis, W. Weng, Y. Davis, A. Nguyen, B. Shapero, M. Jones, D. Million, and T. Martin for participating in the manual component of our synapse identification protocol. We thank E. Liman, I. Foster, K. Chard, P. Rocco-Serra, J. Shepherd, and B. Sabatini for feedback on the manuscript. This work was supported by the National Institute of Mental Health Grant MH107238 to D.B.A., S.E.F., and C.K.

1. M. Mayford, S. A. Siegelbaum, E. R. Kandel, Synapses and memory storage. *Cold Spring Harb. Perspect. Biol.* **4**, a005751 (2012).
2. S. R. Cajal, La fine structure des centres nerveux. *Proc. R. Soc. Lond.* **55**, 444–468 (1894).
3. I. Kupfermann, V. Castellucci, H. Pinsker, E. Kandel, Neuronal correlates of habituation and dishabituation of the gill-withdrawal reflex in Aplysia. *Science* **167**, 1743–1745 (1970).
4. S. J. Martin, P. D. Grimwood, R. G. Morris, Synaptic plasticity and memory: An evaluation of the hypothesis. *Annu. Rev. Neurosci.* **23**, 649–711 (2000).
5. F. Engert, T. Bonhoeffer, Dendritic spine changes associated with hippocampal long-term synaptic plasticity. *Nature* **399**, 66–70 (1999).
6. M. Maletic-Savatic, R. Malinow, K. Svoboda, Rapid dendritic morphogenesis in CA1 hippocampal dendrites induced by synaptic activity. *Science* **283**, 1923–1927 (1999).
7. R. L. Ressler, S. Maren, Synaptic encoding of fear memories in the amygdala. *Curr. Opin. Neurobiol.* **54**, 54–59 (2019).
8. R. G. Phillips, J. E. LeDoux, Differential contribution of amygdala and hippocampus to cued and contextual fear conditioning. *Behav. Neurosci.* **106**, 274–285 (1992).
9. J. E. LeDoux, Emotion circuits in the brain. *Annu. Rev. Neurosci.* **23**, 155–184 (2000).
10. S. Maren, Long-term potentiation in the amygdala: A mechanism for emotional learning and memory. *Trends Neurosci.* **22**, 561–567 (1999).
11. X. Liu *et al.*, Optogenetic stimulation of a hippocampal engram activates fear memory recall. *Nature* **484**, 381–385 (2012).
12. X. Liu, S. Ramirez, S. Tonegawa, Inception of a false memory by optogenetic manipulation of a hippocampal memory engram. *Philos. Trans. R. Soc. Lond. B Biol. Sci.* **369**, 20130142 (2013).
13. S. Ramirez *et al.*, Creating a false memory in the hippocampus. *Science* **341**, 387–391 (2013).
14. S. Ramirez *et al.*, Activating positive memory engrams suppresses depression-like behaviour. *Nature* **522**, 335–339 (2015).
15. R. L. Redondo *et al.*, Bidirectional switch of the valence associated with a hippocampal contextual memory engram. *Nature* **513**, 426–430 (2014).
16. A. J. Rashid *et al.*, Competition between engrams influences fear memory formation and recall. *Science* **353**, 383–387 (2016).
17. T. J. Ryan, D. S. Roy, M. Pignatelli, A. Arons, S. Tonegawa, Memory. Engram cells retain memory under retrograde amnesia. *Science* **348**, 1007–1013 (2015).
18. K. K. Cowansage *et al.*, Direct reactivation of a coherent neocortical memory of context. *Neuron* **84**, 432–441 (2014).
19. M. S. Fanselow, J. E. LeDoux, Why we think plasticity underlying Pavlovian fear conditioning occurs in the basolateral amygdala. *Neuron* **23**, 229–232 (1999).
20. J. LeDoux, The amygdala. *Curr. Biol.* **17**, R868–R874 (2007).
21. A. Attardo, J. E. Fitzgerald, M. J. Schnitzer, Impermanence of dendritic spines in live adult CA1 hippocampus. *Nature* **523**, 592–596 (2015).
22. A. Holtmaat, K. Svoboda, Experience-dependent structural synaptic plasticity in the mammalian brain. *Nat. Rev. Neurosci.* **10**, 647–658 (2009).
23. K. Abdou *et al.*, Synapse-specific representation of the identity of overlapping memory engrams. *Science* **360**, 1227–1231 (2018).
24. W. B. Kim, J. H. Cho, Encoding of discriminative fear memory by input-specific LTP in the amygdala. *Neuron* **95**, 1129–1146.e5 (2017).
25. R. L. Clem, R. L. Huganir, Calcium-permeable AMPA receptor dynamics mediate fear memory erasure. *Science* **330**, 1108–1112 (2010).
26. S. Nabavi *et al.*, Engineering a memory with LTD and LTP. *Nature* **511**, 348–352 (2014).
27. P. Namburi *et al.*, A circuit mechanism for differentiating positive and negative associations. *Nature* **520**, 675–678 (2015).
28. J. H. Choi *et al.*, Interregional synaptic maps among engram cells underlie memory formation. *Science* **360**, 430–435 (2018).
29. C. S. Lai, T. F. Franke, W. B. Gan, Opposite effects of fear conditioning and extinction on dendritic spine remodelling. *Nature* **483**, 87–91 (2012).
30. Z. Xu *et al.*, Fear conditioning and extinction induce opposing changes in dendritic spine remodeling and somatic activity of layer 5 pyramidal neurons in the mouse motor cortex. *Sci. Rep.* **9**, 4619 (2019).
31. C. S. W. Lai, A. Adler, W. B. Gan, Fear extinction reverses dendritic spine formation induced by fear conditioning in the mouse auditory cortex. *Proc. Natl. Acad. Sci. U.S.A.* **115**, 9306–9311 (2018).
32. R. G. Northcutt, Connections of the lateral and medial divisions of the goldfish telencephalic pallium. *J. Comp. Neurol.* **494**, 903–943 (2006).
33. J. Ganz *et al.*, Subdivisions of the adult zebrafish pallium based on molecular marker analysis. *F1000 Res.* **3**, 308 (2014).
34. C. Broglio *et al.*, Hallmarks of a common forebrain vertebrate plan: Specialized pallial areas for spatial, temporal and emotional memory in actinopterygian fish. *Brain Res. Bull.* **66**, 277–281 (2005).
35. M. F. Wullimann, T. Mueller, Teleostean and mammalian forebrains contrasted: Evidence from genes to behavior. *J. Comp. Neurol.* **475**, 143–162 (2004).
36. J. Huisken, J. Swoger, F. Del Bene, J. Wittbrodt, E. H. Stelzer, Optical sectioning deep inside live embryos by selective plane illumination microscopy. *Science* **305**, 1007–1009 (2004).
37. M. Agetsuma *et al.*, The habenula is crucial for experience-dependent modification of fear responses in zebrafish. *Nat. Neurosci.* **13**, 1354–1356 (2010).

38. J. W. Kenney, I. C. Scott, S. A. Josselyn, P. W. Frankland, Contextual fear conditioning in zebrafish. *Learn. Mem.* **24**, 516–523 (2017).
39. A. Lee *et al.*, The habenula prevents helpless behavior in larval zebrafish. *Curr. Biol.* **20**, 2211–2216 (2010).
40. P. Lal *et al.*, Identification of a neuronal population in the telencephalon essential for fear conditioning in zebrafish. *BMC Biol.* **16**, 45 (2018).
41. F. I. Hinz, M. Aizenberg, G. Tushev, E. M. Schuman, Protein synthesis-dependent associative long-term memory in larval zebrafish. *J. Neurosci.* **33**, 15382–15387 (2013).
42. M. Boeckhout, G. A. Zielhuis, A. L. Bredenoord, The FAIR guiding principles for data stewardship: Fair enough? *Eur. J. Hum. Genet.* **26**, 931–936 (2018).
43. A. Valente, K. H. Huang, R. Portugues, F. Engert, Ontogeny of classical and operant learning behaviors in zebrafish. *Learn. Mem.* **19**, 170–177 (2012).
44. Q. Lin *et al.*, Cerebellar neurodynamics predict decision timing and outcome on the single-trial level. *Cell* **180**, 536–551.e17 (2020).
45. W. P. Dempsey *et al*., Fig. 1: Tail flick conditioning (TFC), a robust classical conditioning paradigm for larval zebrafish. Synapse Data Repository. https://doi.org/10.25551/1/1-1YZE. Deposited 6 November 2021.
46. W. P. Dempsey *et al*., Regional synapse gain & loss accompany memory formation in larval zebrafish. Synapse Data Repository. https://doi.org/10.25551/1/1-1JR0. Deposited 6 November 2021.
47. R. Madduri *et al.*, Reproducible big data science: A case study in continuous FAIRness. *PLoS One* **14**, e0213013 (2019).
48. M. D. Wilkinson *et al.*, The FAIR Guiding Principles for scientific data management and stewardship. *Sci. Data* **3**, 160018 (2016).
49. O. Randlett *et al.*, Whole-brain activity mapping onto a zebrafish brain atlas. *Nat. Methods* **12**, 1039–1046 (2015).
50. W. P. Dempsey *et al*., Fig. 2: Neuronal activation within the anterolateral pallium in response to the CS in learner fish and to the US in naïve fish. Synapse Data Repository. https://doi.org/10.25551/1/1-1JP0. Deposited 6 November 2021.
51. K. O. Cho, C. A. Hunt, M. B. Kennedy, The rat brain postsynaptic density fraction contains a homolog of the *Drosophila* discs-large tumor suppressor protein. *Neuron* **9**, 929–942 (1992).
52. A. E. El-Husseini, E. Schnell, D. M. Chetkovich, R. A. Nicoll, D. S. Bredt, PSD-95 involvement in maturation of excitatory synapses. *Science* **290**, 1364–1368 (2000).
53. Ael.-D. El-Husseini *et al.*, Synaptic strength regulated by palmitate cycling on PSD-95. *Cell* **108**, 849–863 (2002).
54. D. A. Fortin *et al.*, Live imaging of endogenous PSD-95 using ENABLED: A conditional strategy to fluorescently label endogenous proteins. *J. Neurosci.* **34**, 16698–16712 (2014).
55. G. G. Gross *et al.*, Recombinant probes for visualizing endogenous synaptic proteins in living neurons. *Neuron* **78**, 971–985 (2013).
56. J. H. Son *et al.*, Transgenic fingRs for live mapping of synaptic dynamics in genetically-defined neurons. *Sci. Rep.* **6**, 18734 (2016).
57. R. M. White *et al.*, Transparent adult zebrafish as a tool for in vivo transplantation analysis. *Cell Stem Cell* **2**, 183–189 (2008).
58. W. P. Dempsey *et al*., Fig. 3: Imaging excitatory synapses in larval zebrafish. Synapse Data Repository. https://doi.org/10.25551/1/1-1JP2. Deposited 6 November 2021.
59. W. P. Dempsey *et al*., Fig. 4: Synapse changes with TFC in larval zebrafish. Synapse Data Repository. https://doi.org/10.25551/1/1-1Z04. Deposited 6 November 2021.
60. W. P. Dempsey *et al*., Fig. 5: Regional differences in synapse formation in the pallium of learner fish. Synapse Data Repository. https://doi.org/10.25551/1/1-1Z06. Deposited 6 November 2021.
61. W. P. Dempsey *et al*., In vivo single-cell labeling by confined primed conversion. *Nat. Methods* **12**, 645–648 (2015).
62. W. P. Dempsey *et al*., Fig. 6. Anatomical correlation of regions of increased neuronal activity and synaptic gain following TFC. Synapse Data Repository. https://doi.org/10.25551/1/1-1Z08. Deposited 6 November 2021.
63. D. S. Roy, S. Muralidhar, L. M. Smith, S. Tonegawa, Silent memory engrams as the basis for retrograde amnesia. *Proc. Natl. Acad. Sci. U.S.A.* **114**, E9972–E9979 (2017).
64. B. Scholl, C. I. Thomas, M. A. Ryan, N. Kamasawa, D. Fitzpatrick, Cortical response selectivity derives from strength in numbers of synapses. *Nature* (2020).
65. A. P. Yiu *et al.*, Neurons are recruited to a memory trace based on relative neuronal excitability immediately before training. *Neuron* **83**, 722–735 (2014).
66. S. Pan, S. R. Mayoral, H. S. Choi, J. R. Chan, M. A. Kheirbek, Preservation of a remote fear memory requires new myelin formation. *Nat. Neurosci.* **23**, 487–499 (2020).
67. S. Tonegawa, M. Pignatelli, D. S. Roy, T. J. Ryan, Memory engram storage and retrieval. *Curr. Opin. Neurobiol.* **35**, 101–109 (2015).
68. S. A. Josselyn, S. Köhler, P. W. Frankland, Finding the engram. *Nat. Rev. Neurosci.* **16**, 521–534 (2015).
69. B. F. Grewe *et al.*, Neural ensemble dynamics underlying a long-term associative memory. *Nature* **543**, 670–675 (2017).
70. A. Beyeler *et al.*, Organization of valence-encoding and projection-defined neurons in the basolateral amygdala. *Cell Rep.* **22**, 905–918 (2018).
71. P. B. Stark, Before reproducibility must come preproducibility. *Nature* **557**, 613 (2018).
72. A. Bugacov *et al.*, Experiences with deriva: An asset management platform for accelerating eScience. *Proc. IEEE Int. Conf. Escience* **2017**, 79–88 (2017).
73. S. A. Sansone *et al.*, Toward interoperable bioscience data. *Nat. Genet.* **44**, 121–126 (2012).
74. V. Trivedi, H. M. T. Choi, S. E. Fraser, N. A. Pierce, Multidimensional quantitative analysis of mRNA expression within intact vertebrate embryos. *Development* **145**, dev156869 (2018).
75. W. P. Dempsey *et al*., Mapping the Dynamic Synaptome. Synapse Data Repository. https://synapse.isrd.isi.edu. Deposited 6 November 2021.